RSC Advances

PAPER

View Article Online
View Journal | View Issue

Check for updates

Cite this: *RSC Adv.*, 2025, **15**, 50775

Electrocoagulation pretreatment for total phosphorus and boron removal in waste lubricating oil regeneration wastewater: efficiency and mechanism

Li-li Shan, *[a] Zong-mei Wu,[a] Ze-bing Zhu,[a] Zhao Tan,[a] Jing-liang Dong,[a] Qiu-zhuo Zhang[b] and Chang-long Pang[c]

Waste lubricating oil regeneration wastewater (WLORW) contains a complex array of pollutants, such as organic oils, ketones, ethers, total phosphorus (TP), and boron (B), whose direct discharge poses significant environmental risks. While previous research has extensively addressed the removal of organic pollutants, oils, and chemical oxygen demand (COD), the treatment of TP and B—similarly harmful yet less studied—has received comparatively limited attention. This gap is particularly pressing in light of China's stringent discharge standards for TP in industrial wastewater. Consequently, this study investigated the efficiency of electrocoagulation as a pretreatment for simultaneously removing TP and B from WLORW on a laboratory scale, employing a two-stage methodology: operational parameters were first optimized using synthetic wastewater *via* an orthogonal experimental design, and then validated with actual wastewater. Under the identified optimal conditions (current density = 15 mA cm^{-2}, initial pH = 7, electrode spacing = 2 cm, treatment time = 30 min), the process achieved removal efficiencies of 79.0% for TP and 13.5% for B from actual WLORW. The primary removal mechanism was identified as flocculant adsorption through both inner-sphere and outer-sphere complexation. Notably, the formation of vivianite within the flocs was observed, indicating a promising avenue for phosphorus resource recovery. Moreover, the hydrogen co-generated at the cathode presents an additional stream of reclaimable energy. In summary, this research provides valuable theoretical insight and practical guidance for scaling up WLORW pretreatment, thereby enhancing the recycling of used lubricating oils and contributing to environmental conservation.

Received 20th October 2025
Accepted 11th December 2025

DOI: 10.1039/d5ra08041j

rsc.li/rsc-advances

Open Access Article. Published on 17 December 2025. Downloaded on 6/19/2026 3:57:09 AM.
This article is licensed under a Creative Commons Attribution-NonCommercial 3.0 Unported Licence.

Introduction

As an indispensable component essential for the operational integrity of mechanical equipment, lubricants are crucial in industrial production and transportation systems. However, lubricants may become contaminated or deteriorate after use, generating high volumes of waste lubricants with significant environmental hazards.[1] Given the global energy crisis and the growing need for environmental protection, recycling waste lubricants has gained prominence.[2] Before regenerating, these lubricants undergo hydrofinishing, vaporization, and alkaline washing to improve their quality.[3] However, these pretreatment processes also generate waste lubricating oil regeneration wastewater (WLORW), which has complex pollutant.

According to the China Lubricant Industry White Paper 2024–2026, the annual apparent consumption of lubricants in China reached 7.8 million tons in 2024.[4] Assuming a 5% waste lubricant content, the annual WLORW volume reaches 380 000 tons. The WLORW contains numerous pollutants (including organic oils, ketones, ethers, total phosphorus (TP), and boron (B)), which can severely pollute the environment through direct discharge or leakage. Consequently, strict adherence to national emission standards is imperative for WLORW management to prevent ecological damage.

Research on the treatment of WLORW remains scarce.[5] For the treatment of similar oily wastewater, techniques such as coagulation,[6] oxidation,[7] electrocoagulation,[8] membrane filtration,[9] and adsorption[10] have been employed. Among these, electrocoagulation is a promising technology, primarily due to its low chemical consumption, multifunctionality, operational safety, ease of operation, and potential for automation.[11–13] Its efficacy is attributed to two concurrent processes: the continuous release of metal ions from the anode and the generation of hydrogen at the cathode. The released metal ions undergo

[a]*School of Civil Engineering and Architecture, East China Jiao Tong University, Nanchang, 330013, China. E-mail: hitshanlili@163.com*

[b]*Shanghai Key Lab for Urban Ecological Processes and Eco-Restoration, Shanghai, 200000, China*

[c]*Jiangxi ZXDH Environmental Protection Industry Technology Institute Co., Ltd., Nanchang, 330000, China*

© 2025 The Author(s). Published by the Royal Society of Chemistry

Open Access Article. Published on 17 December 2025. Downloaded on 6/19/2026 3:57:09 AM. This article is licensed under a Creative Commons Attribution-NonCommercial 3.0 Unported Licence.

hydrolysis and polymerization, forming various metal hydroxo complexes with strong adsorption capacities.[14,15] These complexes entrap aquatic pollutants, facilitating their removal *via* precipitation or flotation. Meanwhile, the hydrogen produced at the cathode offers a potential avenue for energy recovery.[16–18] In our previous study,[5] electrocoagulation achieved a 60.06% oil removal from this wastewater. The process also effectively eliminated recalcitrant organic compounds, and increased the ratio of the five-day biochemical oxygen demand to chemical oxygen demand (BOD_5/COD) by 4.31 times, significantly enhancing the biodegradability of WLORW. However, WLORW also contains higher phosphorus levels. China imposes stringent discharge requirements for TP in industrial effluents, as the Integrated Wastewater Discharge Standard (GB 8978-1996) stipulates that industrial wastewater discharge that complies with level III standards is subject to a TP limit of 5 mg L^{-1} (as phosphorus), which necessitates considering TP removal from this wastewater. Furthermore, water quality analysis revealed elevated B concentrations, posing a challenge requiring resolution regarding whether B presence affects TP removal or not.

In WLORW, TP primarily derives from anti-wear additives such as zinc dialkyldithiophosphates, while B originates from extreme-pressure additives like boric acid esters.[19] Boric acid is primarily a lubricant additive, but it is also applied in detergents and dispersants under ultra-high pressure conditions and as an anti-rust inhibitor.[20] Discharging WLORW directly into water bodies can lead to excessive concentrations of TP and B, which are harmful to aquatic environments. For instance, excessive TP in water bodies (*e.g.*, the critical concentration for eutrophication occurrence in lakes is 0.02 mg per L TP) promotes algal growth, triggering eutrophication and consequently leading to the loss of critical biological habitats.[21] Similarly, B contamination of groundwater poses risks of gastrointestinal and reproductive disorders in humans through long-term exposure.[22] Therefore, developing efficient pretreatment methods for TP and B removal from WLORW is critical.

Electrocoagulation demonstrates efficient TP and B removal. Li *et al.* showed that electrocoagulation achieved a TP removal efficiency of 90% for slaughterhouse wastewater.[23] Similarly, Tuyet *et al.* reported high phosphorus removal (93.12%) using an iron-aluminum electrode reverse electrocoagulation system.[24] Zhang *et al.* electrocoagulated fracturing flowback fluid to remove up to 85% of B.[25] These results demonstrate the technology's adaptability to diverse wastewater matrices. However, research on the pretreatment of WLORW to co-eliminate TP and B before biological treatment remains limited. Therefore, it is necessary to remove TP and B in WLORW simultaneously by electrocoagulation.

To address this gap, we evaluated electrocoagulation for simultaneous TP and B removal during WLORW pretreatment. Using an orthogonal experimental design, we investigated the primary and secondary impacts of control factors (including current density, initial pH, and electrode spacing) on TP and B removal. The removal efficiency in actual wastewater under optimal operating conditions was also examined. To further elucidate the mechanisms behind the removal of inorganic pollutants like TP and B by electrocoagulation, we determined the concentrations of iron ions, formation, and constituents of flocs within the actual WLORW. The findings offer valuable insights for the pretreatment of actual WLORW.

Materials and methods

Materials

The actual WLORW for this study was sourced from Jiangxi Guofu Lubricant Industry Co. Ltd, located in Chihu Industrial Park, Chaisang District, Jiujiang City, Jiangxi Province, China (115°44′56.18″E, 29°46′31.68″N). The company's waste lubricant regeneration process, which includes pretreatment (filtration, impurity removal, and oil-water separation), flash evaporation, thin-film evaporation, molecular distillation, extraction, stripping, and refining, generates 3505 tons of comprehensive wastewater annually. Table S1 details the wastewater quality from waste lubricant regeneration, identifying chemical oxygen demand (80.6 g L^{-1}), oil (1.8 g L^{-1}), TP (12.9 mg L^{-1}), and B (17.5 mg L^{-1}) as the primary pollutants. The collected wastewater samples were refrigerated at 4 °C to preserve the chemical integrity of the compounds during storage. To ensure precise control over initial phosphorus (P) and boron (B) concentrations, as well as the background environmental matrix, this study adopted a two-stage methodology—first optimization with synthetic wastewater, followed by validation using actual WLORW—to evaluate the specific effects of electrochemical parameters on P and B removal. The orthogonal experiments were conducted using synthetic wastewater, which was primarily prepared by dissolving boric acid and sodium tripolyphosphate in deionized water. The elemental concentrations in the synthetic wastewater were based on the TP and B contents detected in the actual WLORW.

Experimental setup and procedures for wastewater treatment

The WLORW was pretreated *via* electrocoagulation to co-remove TP and B. These experiments were performed in a rectangular Plexiglas reactor with dimensions of 100 mm × 50 mm × 130 mm with an effective volume of 500 mL (defined in our previous study).[5] The side walls of the reactor were equipped with parallel slots at variable distances to adjust the position of the electrodes at different intervals. The effective area of the sheet iron cathode and anode electrodes was 50 cm^2 (5 cm × 5 cm × 2 cm). The electrode requires pretreatment prior to use, with specific procedures detailed in the study by Shan.[5] We added Na_2SO_4 as an electrolyte to the WLORW at 3 g L^{-1}, resulting in a conductivity of 8500 μS cm^{-1}. The experiments were conducted by adjusting the initial solution pH, current density, electrode spacing, and treatment time. A DC power (TPR3005-2D, Hong Kong Longwei Instrument Co., Ltd, China) supply generated the required current density, and the initial pH was adjusted using either 2 M H_2SO_4 or 2 M NaOH.

Orthogonal design can evaluate the main and secondary effects of variables, consider parameter interactions, and minimize experimental redundancy, providing a statistically robust framework. Therefore, an orthogonal experimental

 © 2025 The Author(s). Published by the Royal Society of Chemistry

Open Access Article. Published on 17 December 2025. Downloaded on 6/19/2026 3:57:09 AM. This article is licensed under a Creative Commons Attribution-NonCommercial 3.0 Unported Licence.

Table 1 Orthogonal experimental design

	A	B	C	D
Serial number	Current density (mA cm^{-2})	Initial pH	Treatment time (min)	Electrode spacing (cm)
1	10	3	10	1
2	10	5	20	2
3	10	7	30	3
4	10	9	40	4
5	15	3	20	3
6	15	5	10	4
7	15	7	40	1
8	15	9	30	2
9	20	3	30	4
10	20	5	40	3
11	20	7	10	2
12	20	9	20	1
13	25	3	40	2
14	25	5	30	1
15	25	7	20	4
16	25	9	10	3

design (L_{16} (4^4)) was adopted to investigate the simultaneous removal of TP and B from WLORW by electrocoagulation. Four factors were studied at four levels: (10, 15, 20, 25 mA cm^{-2}), pH (3, 5, 7, 9), electrode spacing (1, 2, 3, 4 cm) and treatment time (10, 20, 30, 40 min). Orthogonal experiments were organized using Minitab (version 17) to evaluate the effect of key parameters on TP and B removal efficiency in WLORW. Details of the L_{16} (4^4) orthogonal design, with four levels for each factor, are provided in Table 1. All experiments were repeated three times.

Experimental analysis

Using the molybdenum antimony anti-spectrophotometric method, TP was determined in the wastewater as described in the *Monitoring and Analysis Methods for Water and Wastewater*.[26] A curcumin spectrophotometric method, specified in the Determination of Boron in Water Quality (HJ/T 49-1999), quantified B in the samples. The total iron concentration was determined *via* Lingfiloxanthin Spectrophotometry. These indicators were measured in a UV-vis spectrophotometer (T6 series, Persee Instrument Co., Ltd, Beijing, China). A pH meter (FE28, Mettler-Toledo, Switzerland) and a conductivity meter (FE38, Mettler-Toledo, Switzerland) measured the pH and conductivity, respectively.

The primary constituents of the flocs were examined using X-ray diffraction (XRD, D8 Advance, Bruker, Germany) and Fourier Transform Infrared Spectroscopy (FTIR, iS20, Thermo Scientific Nicolet, USA) techniques. The sizes of the floc images were then quantified using a two-dimensional fractal dimension (D2). Subsequently, the quantity and size of flocs were analyzed with Image-Pro Plus 6.0 software.

Energy consumption and hydrogen generation analysis

The energy efficiency of a treatment process is critically evaluated through its specific energy consumption. Consequently, this metric is essential for the techno-economic analysis of electrocoagulation.

For this purpose, the specific energy consumption per unit volume (SEC) was employed. SEC represents the electrical energy consumed per cubic meter of wastewater treated, which is calculated according to eqn (1).

$$\mathrm{SEC}_{(\mathrm{kWh\ m^{-3}})} = \frac{UIT}{1000V_s} \quad (1)$$

Furthermore, the specific energy consumption per unit pollutant mass (SEEC) was applied. SEEC measures the energy required to remove one kilogram of the target pollutant, as defined in eqn (2).

$$\mathrm{SEEC}_{(\mathrm{kWh\ kg^{-1}})} = \frac{1000UIt}{V(C_0 - C_t)} \quad (2)$$

where U is the reaction voltage (V), I is the reaction current (A), t is the treatment time (h), V is the volume of experimental wastewater (L), and C_0 and C_t are the pollutant concentrations in solution (mg L^{-1}) at the beginning of electrocoagulation and at time t (h), respectively.

The hydrogen energy generation is calculated as follows:[16,17]

$$Q_{H_2} = \frac{I \times A \times t \times H}{F} \quad (3)$$

where Q_{H_2} is the hydrogen generation (mol), I is the applied current per unit area (A m^{-2}), A is the effective surface area of the electrode (m^2), t is the treatment time (s), H is half the molecular weight of hydrogen, and F is the Faraday constant, 96 500 C mol^{-1}. For hydrogen collection in electrocoagulation, the method outlined by Phalakornkule *et al.* serves as the reference, which describes the specific system and procedure employed.[16]

$$E_{H_2} = m(0.244\ \mathrm{MJ\ per\ mole}) \quad (4)$$

© 2025 The Author(s). Published by the Royal Society of Chemistry

Open Access Article. Published on 17 December 2025. Downloaded on 6/19/2026 3:57:09 AM. This article is licensed under a Creative Commons Attribution-NonCommercial 3.0 Unported Licence.

where E_{H_2} denotes the recoverable energy (kJ), and m is the amount of H_2 gas produced (mol).

The TP and B removal efficiencies were calculated as follows:

$$\eta = \frac{C_0 - C_t}{C_0} \times 100\% \quad (5)$$

where C_0 is the initial concentration of TP or B, (mg L^{-1}); C_t is the concentration of TP or B in the supernatant at the end of the electrocoagulation process, (mg L^{-1}).

Statistical analysis

Analysis of variance (ANOVA) determined the degree of influence of controllable factors on experimental results, while the relationship between them was examined using Spearman Correlation. All statistical computations were based on a confidence level of 95%, with a significance level of $p < 0.05$ assumed for separation. Minitab (version 17) and SPSS 26.0 software conducted all data analyses.

Results and discussion

Variance and range analysis

The experiment was conducted using an orthogonal design. The parameters and results of the orthogonal experiment are presented in Fig. 1 and Table 2. The TP and B removal efficiency ranged from 94.0% to 99.2% and 39.8% to 58.1%, respectively

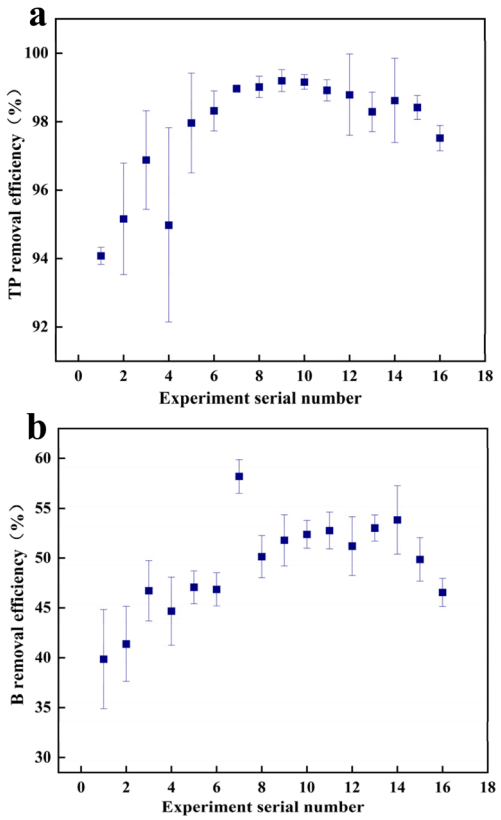

Fig. 1 Removal efficiency variation in orthogonal experiments: (a) total phosphorus (TP); (b) boron (B).

Table 2 Orthogonal experimental results for total phosphorus (TP) and boron (B)[a]

Serial number		A	B	C	D
TP	F	314.7	7.6	10.4	0.5
	P	0.002	0.025	0.007	0.063
	$\bar{K}_{1j}$	95.2	97.4	97.2	97.6
	$\bar{K}_{2j}$	98.6	97.8	97.6	97.9
	$\bar{K}_{3j}$	99.0	98.2	98.3	97.8
	$\bar{K}_{4j}$	98.2	97.6	97.9	97.7
	R	3.9	0.8	1.1	0.2
	Ranking	A > C > B > D			
	Optimal combination	A_3 B_3 C_3 D_2			
B	F	83.2	15.4	37.1	7.8
	P	0.001	0.096	0.044	0.740
	$\bar{K}_{1j}$	43.2	47.9	46.5	50.8
	$\bar{K}_{2j}$	50.6	48.6	47.4	49.3
	$\bar{K}_{3j}$	52.0	51.9	50.6	48.2
	$\bar{K}_{4j}$	50.8	48.1	52.1	48.3
	R	8.9	4.0	5.6	2.6
	Ranking	A > C > B > D			
	Optimal combination	A_3 B_3 C_4 D_1			

[a] Where $\bar{K}_{sj}$ is the sum of the test indicators corresponding to the level of factor s in column j and $\bar{K}_{sj}$ is the mean value of $\bar{K}_{sj}$. The size of $\bar{K}_{sj}$ determines the optimal level of factor j. R_j is the range of factors in column j, which is the index for judging the change of experimental indexes. Generally, the larger the R_j, the more pronounced the factor's influence on column j and the factor's effect on the experiment. Therefore, R_j size can be used to determine the order of factors.

(Fig. 1a and b). ANOVA (Table 2) was used to analyze the significance order of the factors affecting the removal efficiency of TP and B. A sophisticated range analysis (Table 2) investigated the design parameters' effect on TP and B removal and determined the optimal operating conditions. Here, each factor influenced TP and B removal in the sequence A > B > C > D, indicating that current density had the most significant impact, followed by initial pH, electrode spacing, and treatment time. The optimum combination of conditions in the TP removal was A_3 B_3 C_3 D_2 (Table 2), *i.e.*, the optimum process conditions included a current density of 20 mA cm^{-2}, initial pH of 7, electrode spacing of 2 cm, and treatment time of 30 min. For B removal, the combination was A_3 B_3 C_4 D_1 (Table 2), *i.e.*, the optimum process conditions were a current density of 20 mA cm^{-2}, initial pH of 7, electrode spacing of 1 cm, and treatment time of 40 min.

Optimal operation conditions

Fig. 2 depicts the main effect of current density, initial pH, electrode spacing, and treatment time on TP and B removal in the orthogonal experiment of synthetic wastewater. The impacts of current density and initial pH on the removal efficiency were similar. As the current density and initial pH increased, the removal rate initially increased before reducing (Fig. 2). The current density had the most significant effect on the removal because it influenced coagulant generation and bubble size.[27] Within a specific range (10–15 mA cm^{-2}), an increase in current density accelerates the dissolution of the anode and the cathodic reaction, thereby increasing the concentrations of Fe^{3+}

© 2025 The Author(s). Published by the Royal Society of Chemistry

Open Access Article. Published on 17 December 2025. Downloaded on 6/19/2026 3:57:09 AM.
This article is licensed under a Creative Commons Attribution-NonCommercial 3.0 Unported Licence.

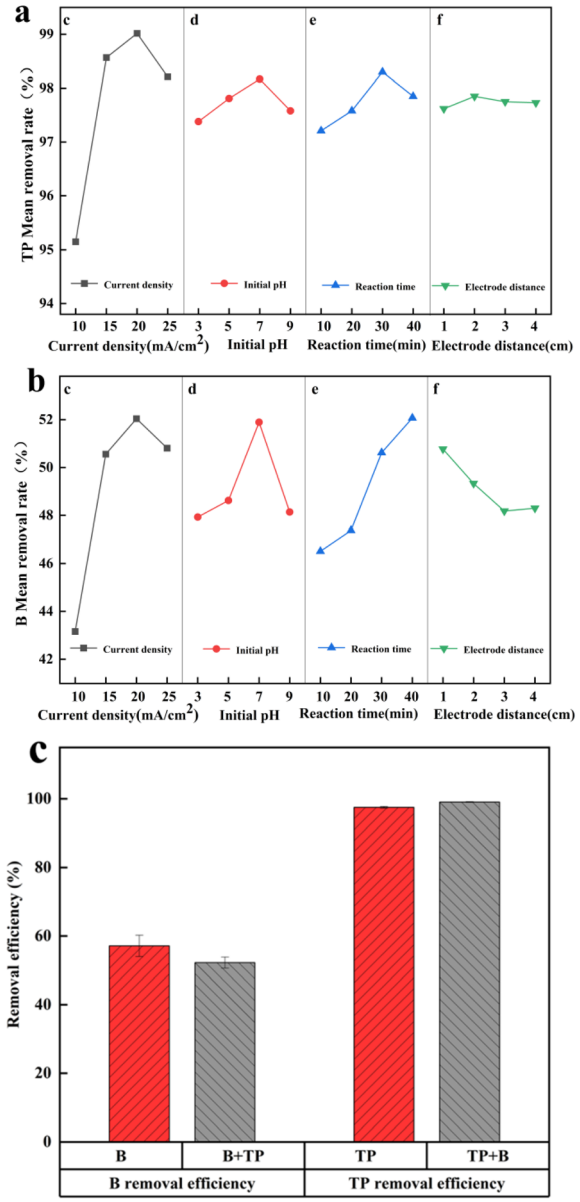

Fig. 2 Mean main effects plot of factors affecting removal efficiency and the interaction diagram showing the effect of total phosphorus (TP)–boron (B) interaction on removal efficiency in synthetic wastewater experiments: (a) total phosphorus (TP); (b) boron (B); (c) TP–B interaction diagram.

and OH^-,[28] which facilitates the removal of TP and B. When the current density is further increased to 20–25 mA cm^{-2}, the removal of phosphorus and boron decreases. This phenomenon may be attributed to either the low concentrations of TP and B in the solution, leading the reaction system to approach saturation,[29] or the increased electrostatic repulsion between TP/B ions and the cathode under a strong electric field,[30] which negatively impacts phosphate and boron complex precipitations. The initial pH affected the hydrogen bubble size at the cathode, impacting the pollutant removal. Hydrogen bubbles at near-neutral pH values aid aggregation and flotation.[31] The pH influence trend on phosphorus and boron removal is similar to that of current density (Fig. 2a and b). Neutral pH conditions exhibit more effective performance, attributable to the fact that iron hydroxides generated on the electrode readily transform into floc species ($Fe(OH)_3$) that facilitate pollutant removal.[32] Iron hydroxide flocs can dissolve under strong alkaline conditions at higher pH values,[33] thus lowering the removal efficiency. During the initial 30 min of electrolysis, the removal of TP and B increased with treatment time (Fig. 2). This occurrence may be that prolonging the treatment time increases the rate of bubble formation and improves the removal of pollutants.[34] After this period, entered a phase of gradual decline (Fig. 2a). The influence of electrode spacing on TP removal was minimal. In contrast, it negatively impacted B removal as the spacing increased.[35,36] Thus, the optimum conditions for TP and B removal were as follows: current density of 20 mA cm^{-2}, initial pH of 7, treatment time of 30 min, and electrode spacing of 2 cm. Furthermore, the interaction between TP and B was also investigated (Fig. 2c). As shown in Fig. 2c, the interaction between TP and B influences their removal efficiencies. Specifically, TP inhibits B removal, while B slightly promotes TP removal. Because the removal efficiency at a current density of 20 mA cm^{-2} was only 0.45% higher than at 15 mA cm^{-2}, we selected the experimental condition of 15 mA cm^{-2} to reduce energy consumption (Table S2 lists the data on removal efficiency *versus* energy consumption). Therefore, the subsequent electrocoagulation actual wastewater experiment conditions for wastewater treatment were current density of 15 mA cm^{-2}, initial pH of 7, treatment time of 30 min, and electrode spacing of 2 cm.

Pollutant removal efficiency in WLORW

Based on orthogonal experimental results, we investigated the performance of electrocoagulation in removing TP and B from actual wastewater under a current density of 15 mA cm^{-2}, an initial pH of 7, a treatment time of 30 min, and an electrode spacing of 2 cm. Fig. 3a and b displays the removal efficiencies of TP and B in actual WLORW. The removal efficiencies of both pollutants increased with treatment time. A rapid removal phase for TP and B was observed within the first 15 min, after which the removal rate slowed down markedly. Our previous study indicated that more flocs formed before 15 min, thereby promoting the removal of the target contaminants.[5] The formation of these flocs depends on the release of iron ions. As the treatment proceeded, the release of iron ions slowed down significantly, falling far below the theoretical iron production (Fig. 3c). This can be primarily attributed to the passivation of the iron anode surface.[15] The extent of passivation further influences the frequency required for replacing the iron electrodes. Compared to the orthogonal experimental setup for synthetic wastewater, the electrocoagulation in actual wastewater was significantly more effective in removing TP than B. Besides, the removal efficiencies for TP and B from actual WLORW were reduced to varying degrees, with a slight increase in specific energy consumption. This deduction may be attributed to the complex composition of actual WLORW,[5] where organic compounds interfere with the removal of TP and B. Our

Open Access Article. Published on 17 December 2025. Downloaded on 6/19/2026 3:57:09 AM.
This article is licensed under a Creative Commons Attribution-NonCommercial 3.0 Unported Licence.

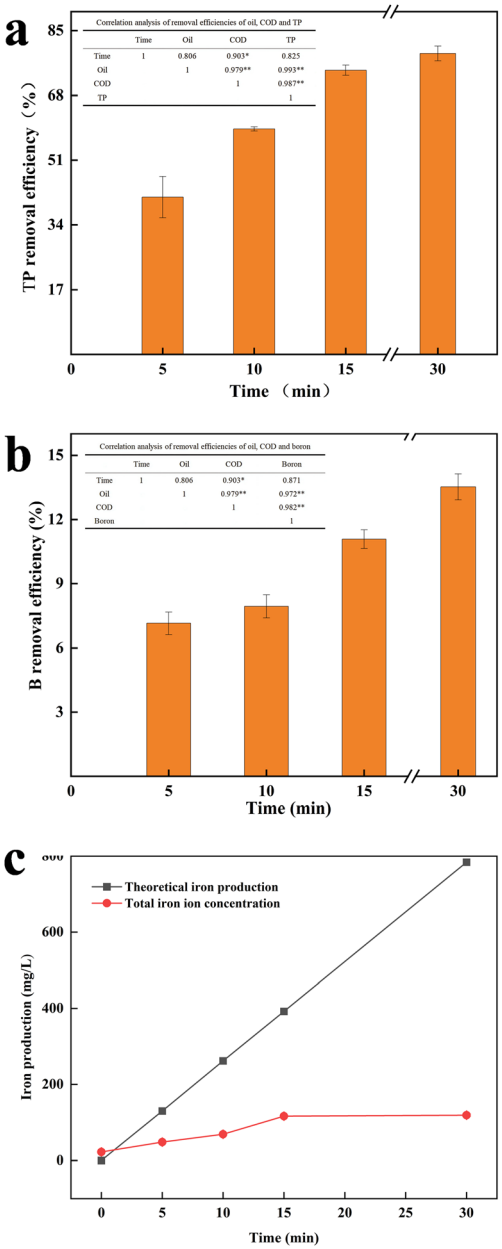

Fig. 3 Removal efficiency of total phosphorus (TP) and boron (B) in actual wastewater and release of iron ions: (a) total phosphorus (TP); (b) boron (B); (c) iron production.

previous study demonstrated that WLORW is a high-strength, complex oily wastewater containing organic substances such as ketones, ethers, amides, and phenolic compounds.[5] Electrocoagulation has proven effective, achieving excellent oil removal and satisfactory COD removal.[5] Considering the impact of wastewater complexity on TP and B removal, a correlation analysis was performed between the removal efficiencies of TP/B and those of oils/COD. The results indicated a statistically significant positive correlation between TP removal and the removal of both oils and COD (Fig. 3a and its embedded table). A similar positive correlation was observed for B removal, suggesting that oils and COD substantially influence the removal of both TP and B in this wastewater (Fig. 3b and its embedded table). Moreover, according to the literature, the presence of suspended solids (SS) in wastewater has been reported to enhance COD removal efficiency, which is attributed to the formation of colloidal coagulants comprising SS and polymeric iron hydroxides.[37] Given the significant correlation established in this study between TP/B removal and COD removal, the reported effect of SS likely also facilitates the co-removal of TP and B. Moreover, as demonstrated in section "Optimal operation conditions", the interaction between TP and B also influences their removal efficiencies. The TP removal from actual wastewater reached 79.0% in 30 min (Fig. 3a), whereas B removal was only 13.5% in 30 min (Fig. 3b). This observation is likely due to the complex composition of the actual wastewater, which significantly impacts boron removal. This finding aligns with the research by Zhang *et al.*,[25] where electrolysis for 30 min at a current density of 20 mA cm^{-2} resulted in only approximately 20% boron removal in boron-containing actual wastewater. Whereas, when the current density was elevated to 46.3–57.2 mA cm^{-2}, the removal efficiency enhanced to approximately 50%, while achieving 84% removal required prolonged electrolysis of 90 min. However, considering energy consumption and the preferential removal of phosphorus, the current density was not increased in this study. The specific energy consumption for TP and B removal was 0.43 and 1.89 kWh kg, respectively. The discrepancy in removal efficiency may be attributed to Ca^{2+} and Mg^{2+} in the wastewater, which hinder the formation of iron hydroxide flocs.[36] Additionally, other anions (such as SO_4^{2-}) likely in the wastewater might inhibit the iron electrode dissolution when highly concentrated, thus precipitating into an insulating layer on the electrodes.[38,39] This occurrence could lower the current efficiency and slightly increase the specific energy consumption.

In addition, generating hydrogen gas during electrocoagulation is a promising green energy source.[6] Elsewhere, Phalakornkule *et al.* indicate that converting hydrogen gas into electrical energy can offset 5.8–13.0% of the energy required for electrocoagulation.[16] Under optimal experimental conditions, treating 0.5 L of waste lubricating oil regeneration wastewater can produce 0.007 moles of H_2, with an electrical energy consumption of 4.5 kWh m^3. This estimation equates to producing 14 moles of H_2 for every metric ton of waste lubricating oil used for regenerating wastewater, sufficient to generate 0.949 kWh of electrical power.

$$Q_{H_2} = \frac{150 \times 0.005 \times 1800 \times 0.5}{96500} = 0.007 \text{ mole}$$

The hydrogen production rate was quantified at 14 mol per cubic meter of treated wastewater. Based on this yield, the corresponding amount of recoverable energy from the H_2 gas can be calculated.

$$E_{H_2} = 14 \text{ moles} \times 0.244 \text{ MJ per mole} = 3.416 \text{ MJ}$$

Consequently, the recoverable energy from the H_2 generated during electrocoagulation is equivalent to 0.949 kWh per m^3 of

© 2025 The Author(s). Published by the Royal Society of Chemistry

Open Access Article. Published on 17 December 2025. Downloaded on 6/19/2026 3:57:09 AM.
This article is licensed under a Creative Commons Attribution-NonCommercial 3.0 Unported Licence.

treated wastewater (based on the conversion factor of 3.6 MJ = 1.0 kWh).

$$\text{SEC}\ \left(\text{kWh m}^{-3}\right) = \frac{6 \times 0.75 \times 0.5}{1000 \times 0.0005} = 4.5\ \ \left(\text{kWh m}^{-3}\right)$$

where SEC is the specific energy consumption per unit volume (kWh m^3), defined as the electrical energy required to treat one cubic meter of wastewater.

Quantity, floc size, and constituent analyses

The size and strength of flocs are essential in evaluating the ability of electrocoagulation technology to remove pollutants from wastewater.[40] Therefore, we analyzed the characteristics of flocs in the electrocoagulation of actual WLORW. Floc growth involves formation, growth, and breakage stages.[6] Flocs are formed through the electrolytic reaction between the electrodes during electrocoagulation. The quantity and size of the flocs were analyzed after they had stabilized for 30 min (Fig. 4). The sizes of the flocs were ≤100 μm (mean = 5.53 μm). Most flocs fell within the 5–10 μm range, with flocs larger than 32 μm constituting 10% of the total flocs (Fig. 4), indicating that larger flocs had disintegrated into smaller ones.[9] Terminating the experiment at this point can yield favorable results while minimizing energy loss. Our previous study shows that forming these flocs is closely associated with the electrolysis of iron and the zeta potential within the wastewater.[5] Then, in the growth phase, the iron plate anode continuously releases ions through electrolysis, which fosters the formation and growth of hydroxide flocs.

Fig. 5 presents the FTIR and XRD patterns of the flocs. The FTIR spectrum revealed –OH group stretch vibrations within 3429 – 3699 cm^{-1}, O–H–O bending vibrations at 1629 cm^{-1} associated with water molecules, phosphate absorption peaks between 900 – 1200 cm^{-1}, and –Fe–O– vibrations at 620 cm^{-1} (Fig. 5a). The XRD pattern indicated that after 30 min of electrolysis, the primary constituents of the flocs were hydroxyl phosphate iron compounds and hydrated ferrous phosphates (Fig. 5b)). The diffraction peaks observed for the flocs at 11.220°, 18.216°, and 32.729° closely match the characteristic

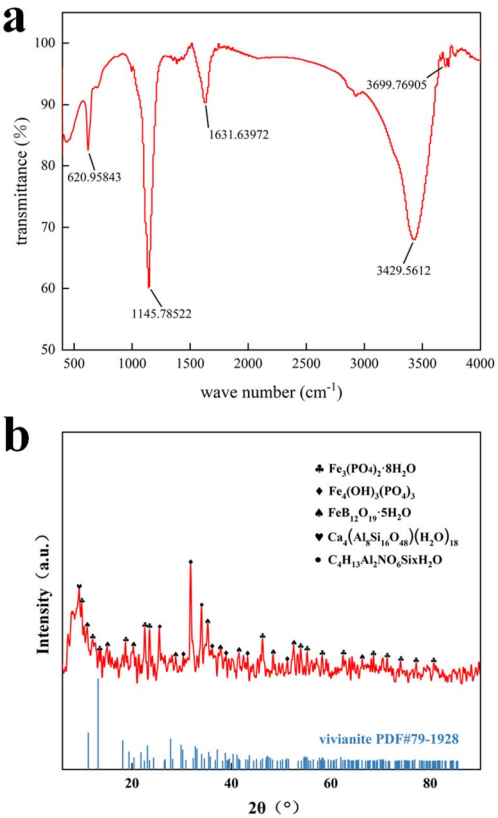

Fig. 5 Fourier Transform Infrared Spectroscopy (FTIR) and X-ray diffraction (XRD) of the main constituents of flocs: (a) FTIR; (b) XRD.

peaks of the vivianite PDF reference card, with corresponding peak shapes showing good agreement. This correspondence confirms the formation of vivianite crystals within the electrocoagulation flocs, a product which is of significant interest for resource recovery due to its economic value. In addition to vivianite, other Fe(III)–P compounds, such as $Fe_4(OH)_3(PO_4)_3$, $FeH_2P_3O_{10}$, $Fe_2(HPO_3)_3$ and $Fe_3(PO_4)_2{\cdot}4H_2O$, are present in the flocs. Furthermore, compounds consistent with iron borate hydrate phases are also identified in the floc composition.

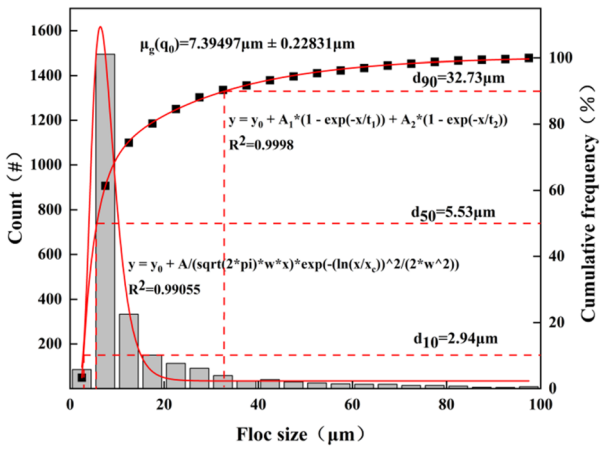

Fig. 4 Floc size and quantity after stabilization.

Removal mechanism of pollutants from WLORW

Generally, electrocoagulation of pollutants involves several processes: electrolytic reactions on the electrode, floc formation in the solution, pollutant (soluble or colloidal) adsorption by flocculants, and pollutant removal through precipitation or air flotation. The electrolytic reactions at the electrode surface are the primary mechanism responsible for forming metal hydroxides, which act as flocculants in the solution. In the electrocoagulation process for phosphorus removal using iron electrodes, the resulting flocs may include not only iron hydroxides but also ferrous phosphate and iron hydroxyl phosphate species.[18] Phosphate ions (PO_4^{3-}) exhibit strong affinity for $Fe_x(OH)_y^{(3x-y)}$ (s). In solution, PO_4^{3-} undergoes ligand exchange with –OH groups, leading to the adsorption of phosphate ions onto metal oxide surfaces through inner-sphere complexation. When water molecules remain present between

Open Access Article. Published on 17 December 2025. Downloaded on 6/19/2026 3:57:09 AM. This article is licensed under a Creative Commons Attribution-NonCommercial 3.0 Unported Licence.

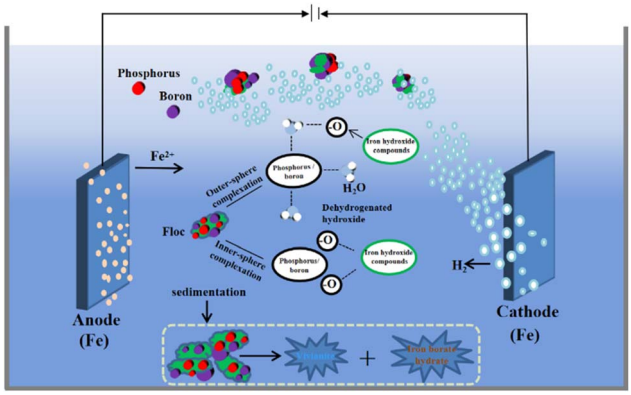

Fig. 6 The mechanism of total phosphorus (TP) and boron (B) removal from the WLORW by electrocoagulation.

the adsorbed phosphate ions and the hydroxide surface, the interaction is referred to as outer-sphere complexation.

In this study, the removal mechanism of TP in actual WLORW may be described as follows (Fig. 6) : (i) the formation of iron phosphate complexes, $Fe(OH)_{3-x}(PO_4)_{x(s)}$, *via* inner-sphere complexation.[41] These complexes can adsorb onto positively charged Fe(III) hydrolysates or serve as nucleation sites for these hydrolysates. (ii) PO_4^{3-} adsorb onto Fe(III) hydrolysates through outer-sphere complexation.[41] As the treatment time extends, Fe(III) hydrolysis products are gradually converted into hydroxyl complexes and ferrous phosphate, thereby removing phosphates *via* adsorption. Consequently, the primary components of the generated sludge include $Fe(OH)_3$ and adsorbed iron-phosphorus compounds such as vivianite. Regarding the disposal of this iron-phosphorus sludge, its subsequent resource recovery is of significant importance.[42,43] The B removal during electrocoagulation is similar to that of TP, with B primarily adsorbing onto amorphous iron hydroxide (Fig. 6). As a Lewis acid, boric acid has electrostatic properties and forms complexes with $Fe(OH)_3$ on the outer and inner layers, where the compound effect of inner and outer spheres occurs.[11,44] Also, hydrogen bubbles generated at the cathode help lift the flocs to the water surface. The interaction between bubbles and unstable flocs causes the flocs to float upward while heavier flocs sink to the bottom, ultimately completing the pollutant removal. The treated wastewater can be easily separated from the suspended solids, effectively removing TP and B.

Conclusions

This study demonstrates that electrocoagulation effectively removes TP and B from WLORW. Orthogonal experiments with synthetic wastewater, evaluating removal efficiency and SEC, identified optimal parameters: current density = 15 mA cm^{-2}, initial pH = 7, electrode spacing = 2 cm, and treatment time = 30 min. Under these conditions, removal rates of 79.0% for TP and 13.5% for B were achieved with actual WLORW. The primary mechanism is complexation with *in situ* generated Fe(III) species *via* inner- and outer-sphere interactions. Specifically, TP removal occurs through ligand exchange forming iron phosphate complexes (*e.g.*, $Fe(OH)_{3-x}(PO_4)_x(s)$) or adsorption onto Fe(III) hydrolysates. Notably, vivianite formation within the flocs indicates a pathway for P recovery. B removal follows a similar route, primarily through adsorption onto amorphous $Fe(OH)_x$. Furthermore, the co-generated H_2 constitutes a reclaimable energy source, enhancing process sustainability.

Author contributions

All authors contributed to the study conception and design. Conceptualization and methodology were performed by Ze-bing Zhu and Li-li Shan. The investigation and first draft of the manuscript was written by Zong-mei Wu. The writing – review & editing and funding acquisition were performed by Li-li Shan and Ze-bing Zhu. The investigation and data curation was performed by Zhao Tan. The editing was performed by Qiu-zhuo Zhang. The investigation was performed by Chang-long Pang. The editing was performed by Jing-liang Dong. All authors commented on previous versions of the manuscript, and all authors read and approved the final manuscript.

Conflicts of interest

The authors declare no competing interests.

Data availability

The data that support the findings of this study are available from the corresponding author upon reasonable request.

Supplementary information (SI) is available. See DOI: https://doi.org/10.1039/d5ra08041j.

Acknowledgements

This research was funded by the National Natural Science Foundation of China (52460009), Science and Technology Research Project of Jiangxi Provincial Department of Education (GJJ2200652, GJJ2200645), the Natural Science Foundation of Jiangxi Province (20242BAB25314, 20232BAB204096) and Shanghai Key Laboratory for Urban Ecological Processes and Eco-Restoration (SHUES2023A06). We thank International Science Editing (http://www.internationalscienceediting.com) for editing this manuscript.

References

1 B. Yu, Y. Peng, H. Gong and Y. Liu, *Sep. Purif. Technol.*, 2023, **312**, 123402.
2 R. Maceiras, V. Alfonsin and F. J. Morales, *Waste Manag.*, 2017, **60**, 351–356.
3 R. Feizi, M. R. Khavari Kashani, N. Jaafarzadeh, G. Varank, F. Bazipur and F. Ghanbari, *Water, Air, Soil Pollut.*, 2023, **234**, 777.
4 Lub Top Market Research Center China Lubricant Information Network, *2024-2026 China Lubricant Industry* White Paper, 2024.

© 2025 The Author(s). Published by the Royal Society of Chemistry

Open Access Article. Published on 17 December 2025. Downloaded on 6/19/2026 3:57:09 AM. This article is licensed under a Creative Commons Attribution-NonCommercial 3.0 Unported Licence.

5 L.-l. Shan, Z. Tan, Y. Chen, R.-s. Wang, M. Zhang, C.-l. Pang, Y.-H. Cui, Z.-m. Liao, H.-q. Ma and Z.-b. Zhu, *Environ. Sci. Pollut. Res.*, 2023, **30**, 106421–106430.
6 T. Harif and A. Adin, *Water Res.*, 2011, **45**, 6195–6206.
7 Y. M. Chen, W. M. Jiang, Y. Liu and Y. Kang, *Chemosphere*, 2020, **250**, 126128.
8 J. Ano, A. S. Assémian, Y. A. Yobouet, K. Adouby and P. Drogui, *Process Saf. Environ. Prot.*, 2019, **129**, 184–195.
9 M. Nasrullah, L. Singh, S. Krishnan, M. Sakinah, D. M. Mahapatra and A. W. Zularisam, *J. Water Proc. Eng.*, 2020, **33**, 101114.
10 J. Duan and J. Gregory, *Adv. Colloid Interface Sci.*, 2003, **100–102**, 475–502.
11 M. A. Sari and S. Chellam, *J. Colloid Interface Sci.*, 2015, **458**, 103–111.
12 J. Y. Lin, A. Raharjo, L. H. Hsu, Y. J. Shih and Y. H. Huang, *Water Res.*, 2019, **155**, 362–371.
13 G. P. Bhoi, K. S. Singh and D. A. Connor, *Water Environ. Res.*, 2023, **95**, e10847.
14 M. Ingelsson, N. Yasri and E. P. L. Roberts, *Water Res.*, 2020, **187**, 116433.
15 R.-s. Wang, L.-l. Shan, Z.-b. Zhu, Z.-q. Liu, Z.-m. Liao and Y.-h. Cui, *Chem. Eng. Process. Process Intensif.*, 2025, **209**, 110192.
16 C. Phalakornkule, P. Sukkasem and C. Mutchimsattha, *Int. J. Hydrogen Energy*, 2010, **35**, 10934–10943.
17 K. S. Hashim, A. Shaw, R. Al Khaddar, M. O. Pedrola and D. Phipps, *J. Environ. Manage.*, 2017, **196**, 224–233.
18 P. I. Omwene and M. Kobya, *Process Saf. Environ. Prot.*, 2018, **116**, 34–51.
19 Z. Jiang, Q. Chu, H. Yang, R. Zhao, Y. Yu, M. Wang and R. Liu, *Process Saf. Environ. Prot.*, 2021, **148**, 980–991.
20 J. C. O. Santos, R. A. Almeida, M. W. N. C. Carvalho, A. E. A. Lima and A. G. Souza, *J. Therm. Anal. Calorim.*, 2019, **137**, 1463–1470.
21 X. Chen, X. Song, W. Chen and T. Ao, *Environ. Technol.*, 2024, **45**, 3381–3395.
22 J. Y. Lin, N. N. N. Mahasti and Y. H. Huang, *J. Hazard. Mater.*, 2021, **407**, 124401.
23 G. Li, B. Zheng, W. Zhang, Q. Liu, M. Li and H. Zhang, *Sustainability*, 2024, 16.
24 N. T. Tuyet, V. D. Nguyen, N. T. Nguyet, R. Balasubramani and N. T. Nghia, *Environ. Res. Commun.*, 2024, **6**, 105005.
25 Y. Zhang, X. Chen, M. Dong, M. Li, C. Wang and Y. Zhang, *Desalination Water Treat.*, 2024, **317**, 100127.
26 The State Environmental Protection Administration, *The Water and Wastewater Monitoring Analysis Method Editorial Board, Water and Wastewater Monitoring Analysis method*, China Environmental Science Press, 4th edn, Beijing, 2002, (in Chinese).
27 P. Asaithambi, B. Sajjadi, A. R. Abdul Aziz and W. M. A. B. Wan Daud, *Process Saf. Environ. Prot.*, 2016, **104**, 406–412.
28 Z. Wang, X. An, P. Wang, X. Du, X. Hao, X. Hao and X. Ma, *Environ. Sci. Pollut. Res.*, 2023, **30**, 50567–50581.
29 Y. Liu, J. Zhou, Z. Zhang, X. Li, D. Yang, Y. Chang, H. Xu and W. Yan, *Chem. Eng. J.*, 2025, **512**, 162468.
30 Y. Takabe, N. Ota, M. Fujiyama, Y. Okayasu, Y. Yamasaki and M. Minamiyama, *Sci. Total Environ.*, 2020, **706**, 136090.
31 B. Merzouk, M. Yakoubi, I. Zongo, J. P. Leclerc, G. Paternotte, S. Pontvianne and F. Lapicque, *Desalination*, 2011, **275**, 181–186.
32 A. Mielcarek, K. Ł. Bryszewski, J. Rodziewicz, K. Kłobukowska and W. Janczukowicz, *Energies*, 2024, **17**.
33 D. D. Nguyen, Y. S. Yoon, X. T. Bui, S. S. Kim, S. W. Chang, W. Guo and H. H. Ngo, *Environ. Sci. Pollut. Res.*, 2017, **24**, 25441–25451.
34 N. Muhammad Niza, M. S. Yusoff, M. A. A. Mohd Zainuri, M. I. Emmanuel, A. Mohamed Hussen Shadi and M. A. Kamaruddin, *J. Water Proc. Eng.*, 2020, **36**, 101282.
35 P. T. P. Aryanti, F. A. Nugroho, C. Phalakornkule and A. Kadier, *J. Environ. Chem. Eng.*, 2024, **12**(6), 114124.
36 M. Chen, O. Dollar, K. Shafer-Peltier, S. Randtke, S. Waseem and E. Peltier, *Water Res.*, 2020, **170**, 115362.
37 J. Ding, K. Wang, S. Wang, Q. Zhao, L. Wei, H. Huang, Y. Yuan and D. D. Dionysiou, *Chem. Eng. J.*, 2018, **344**, 34–41.
38 K. S. Hashim, R. Al Khaddar, N. Jasim, A. Shaw, D. Phipps, P. Kot, M. O. Pedrola, A. W. Alattabi, M. Abdulredha and R. Alawsh, *Sep. Purif. Technol.*, 2019, **210**, 135–144.
39 D. T. Moussa, M. H. El-Naas, M. Nasser and M. J. Al-Marri, *J. Environ. Manage.*, 2017, **186**, 24–41.
40 Y. Liu, X. Zhang, W. Jiang, M. Wu and Z. Li, *Chem. Eng. J.*, 2021, **417**, 129310.
41 S. S. Lam, R. K. Liew, A. Jusoh, C. T. Chong, F. N. Ani and H. A. Chase, *Renew. Sustain. Energy Rev.*, 2016, **53**, 741–753.
42 H. Li, Z. Xu, T.-Y. Chen, F. Meng, H. Chen, C. Liu, G. Qiu and C. Feng, *J. Hazard. Mater.*, 2025, **495**, 139050.
43 S. Lu, W. Zeng, Q. Gong, J. Zhang, X. Peng, X. Yu and Y. Peng, *Process Saf. Environ. Prot.*, 2024, **190**, 381–394.
44 D. Chorghe, M. A. Sari and S. Chellam, *Water Res.*, 2017, **126**, 481–487.

© 2025 The Author(s). Published by the Royal Society of Chemistry